Strong optical nonlinearity in strain-induced laterally ordered InGaAs quantum wires on GaAs (311) A substrate

ARTICLE *in* JOURNAL OF APPLIED PHYSICS · SEPTEMBER 2005

Impact Factor: 2.18 · DOI: 10.1063/1.2039999

11 AUTHORS, INCLUDING:

Georgiy Tarasov
University of Arkansas
145 PUBLICATIONS **808** CITATIONS
SEE PROFILE

V. V. Strelchuk
National Academy of Sciences of Ukraine
249 PUBLICATIONS **435** CITATIONS
SEE PROFILE

Dorel Guzun
University of Arkansas
26 PUBLICATIONS **208** CITATIONS
SEE PROFILE

Matthew Johnson
University of Oklahoma
138 PUBLICATIONS **2,580** CITATIONS
SEE PROFILE

Strong optical nonlinearity in strain-induced laterally ordered $In_{0.4}Ga_{0.6}As$ quantum wires on GaAs (311)A substrate

Yu. I. Mazur,[a] Zh. M. Wang, G. G. Tarasov,[b] H. Wen, V. Strelchuk,[b] D. Guzun, M. Xiao, and G. J. Salamo
Physics Department, University of Arkansas, Fayetteville, Arkansas 72701

T. D. Mishima, Guoda D. Lian, and M. B. Johnson
Center for Semiconductor Physics in Nanostructures, University of Oklahoma, Norman, Oklahoma 73019

(Received 1 February 2005; accepted 29 July 2005; published online 13 September 2005)

Strain-induced laterally ordered $In_{0.4}Ga_{0.6}As$ on (311)A GaAs template quantum wires have been fabricated and identified with cross-section transmission electron microscopy technique to be of average length $\sim 1\ \mu m$, and on average width and height of 23 and 2 nm, respectively, under InGaAs coverage of six monolayers. The photoluminescence spectrum of a sample demonstrates unusually strong optical nonlinearity even at moderate excitation densities. The excitonic peak energy blueshifts by ~ 25 meV without essential contribution of the quantum wire excited states at elevating excitation density. Strong decrease of the polarization anisotropy and increase of the energy of excitonic photoluminescence are attributed to a combined action of the phase-space filling effects and the screening of the internal piezoelectric field by free carriers. © *2005 American Institute of Physics*. [DOI: 10.1063/1.2039999]

I. INTRODUCTION

Recently, self-assembled quantum wires (QWRs) of various shapes, sizes, densities, optical and electronic properties have been fabricated[1–5] promising further advances in optoelectronic devices (e.g., lasers[6] and modulators[7]). The two-dimensional (2D) confinement inherent to QWRs produces a singularity in the density of states (DOS).[8] The narrowing of the DOS leads to a lower excitation threshold for phase-space filling in QWRs,[9] thus enhancing nonlinear optical effects important for applications in optical communications.

One of the interesting optical features associated with strain-driven self-assembled QWRs is an intrinsic photoluminescence (PL) polarization anisotropy due to the complicated structure of the valence band at the center of the Brillouin zone.[10] The complex, nontetragonal strain deformation, developed due to the lattice mismatch, splits the degenerated valence band into a complicated subband structure,[11,12] resulting in both the polarization anisotropy[13] and lateral piezoelectric fields.[14] These fields could be important for optical nonlinearities due to screening of the field as well as the range of the field away from the strained layers. Indeed, it has been demonstrated in a series of (110) InAs/GaAs QWR structures that in high excitation density PL experiments produce a pronounced (up to 22 meV) blueshift of the PL lines, simultaneously with a clear reduction of the linewidth.[14] In these experiments, the observed blueshift and linewidth reduction were attributed to the screening of the internal piezoelectric fields by photogenerated carriers. In addition, the photoexcited carriers could also result in the screening and eventually bleaching of the exciton binding energy in QWRs. Enhancement of the optical nonlinearity has been revealed also in quasiplanar sidewall QWRs on GaAs (311)A substrate by means of continuous-wave PL.[15]

While screening would seem to explain the optical behavior of QWRs under high-density optical illumination, this is not the case due to the fact that there exist numerous contradictory observations of the PL peak energy behavior under high optical excitation density for strained QWR systems: from a sizable redshift ~ 10 meV,[16] virtually no shift[17,18] to a sizable blueshift [~ 25 meV (Ref. 19); 17 meV (Ref. 20)]. It is clear that different mechanisms can contribute to this behavior at high excitation density such as band filling, excitonic correlations, band-gap renormalization, and disorder. In fact, the nature of the PL peak shift and the polarization anisotropy properties in QWR systems are not yet well understood in spite of good potential for applications in low-threshold lasers and exotic light modulators.

In this study, we examine the nonlinear optical properties of strain-induced laterally ordered (SILO) $In_{0.4}Ga_{0.6}As$ QWRs on the GaAs (311)A substrate. The QWRs have been unambiguously identified with transmission electron microscopy (TEM) and PL measurements carried out at the moderate excitation optical densities. We demonstrate the existence of interesting excitation and temperature-dependent polarization anisotropy and a strong blueshift in the PL spectrum coming from the SILO QWRs that give evidence for strong nonlinear optical effects.

II. SAMPLES AND EXPERIMENTAL DETAILS

The QWR structures for this study were grown by molecular-beam epitaxy on a GaAs(311)A substrate. The GaAs wafer was first covered with a buffer layer of 0.5-μm thickness grown at 600 °C. For the (In,Ga)As deposition, the substrate temperature was reduced to 540 °C, the

[a]Electronic mail: ymazur@uark.edu
[b]On leave from Institute of Semiconductor Physics, National Academy of Sciences of Ukraine, Prospect Nauki 45, 03028 Kiev, Ukraine.

highest temperature at which In desorption can be considered insignificant. The As beam equivalent pressure was kept constant at 1×10^{-5} Torr for all the structures.

The surface evolution of mismatched (In,Ga)As on the GaAs(311)A substrate provides unique possibilities for nanostructure growth. Depending on the In content and the (In,Ga)As coverage, (In,Ga)As/GaAs(311)A quantum wells (QWs), QWRs, or quantum dots (QDs) can be produced.[2,21,22] For the case of growth of $In_{0.4}Ga_{0.6}As$ on GaAs(311)A templates, we observed a layer-by-layer 2D growth mode up to 4.0 ML (monolayer) of coverage. The deposition of 6.0 ML of $In_{0.4}Ga_{0.6}As$ leads to fairly uniform QWRs along the $[2\bar{3}\bar{3}]$ direction. Further deposition up to 10.0-ML $In_{0.4}Ga_{0.6}As$ produces QDs superimposed on a corrugated wetting layer. Therefore, the (In,Ga)As growth mode on GaAs(311)A starts from 2D, goes through one dimensional (1D), and finally leads to zero dimensional (0D). Generally, a direct transition from 2D to 0D growth occurs for (In,Ga)As growth on a GaAs(100) substrate although elongated islands were also observed.[23,24]

Two samples with $In_{0.4}Ga_{0.6}As$ layer of 4.0 and 6.0 ML chosen for optical investigations were capped with a 50-nm GaAs layer before PL and TEM measurements were carried out. The TEM analysis was performed using a JEOL JEM-2000FX microscope operated at 200 kV. For both plan-view and cross-section analyses the specimens were prepared using mechanical thinning and dimpling, followed by 2-keV Ar^+-ion milling with the specimen cooled with liquid nitrogen. TEM images give direct evidence that the 4.0-ML sample is a normal $In_{0.4}Ga_{0.6}As$ quantum well in a GaAs(311)A matrix, although some surface corrugation along $[2\bar{3}\bar{3}]$ exists. The intrinsic corrugation on GaAs(311)A is around 0.34 nm. The short-period corrugation of the $In_{0.4}Ga_{0.6}As$ layer is about 5 nm by width and 0.4 nm by height. For the 6.0-ML sample, QWR confinement is expected as a result of the strain-driven 1D self-assembly. Figure 1(a) shows a plan-view TEM image along the [311] direction. A two-beam 022 dark-field (DF) condition was chosen to obtain this image, because of its sensitivity to a strain field in the direction. The (In,Ga)As QWRs with a distinct contrast are seen to be self-assembled, with an average QWR length of ~1 μm and an average center-to-center distance between adjacent QWRs of the order of ~35 nm. The fast Fourier-transform (FFT) spectrum [Fig. 1(b)] calculated for Fig. 1(a) indicates the overall QWR direction to be the $[2\bar{3}\bar{3}]$ direction. This assignment is confirmed also by two kinds of cross-sectional TEM (X-TEM) images: the 002 DF made along the $[01\bar{1}]$ direction [Fig. 1(c)] and the 622 DF made along the $[2\bar{3}\bar{3}]$ direction [Fig. 1(d)]. Additionally, using X-TEM images the average wire width and height were found to be of 23 and 2 nm, respectively. The TEM analysis indicates that the perfect strained QWRs of high density are produced during (In,Ga)As deposition on GaAs(311)A.

The PL measurements were performed in a variable temperature of 8–300-K closed-cycle helium cryostat. The 532-nm line from a doubled Nd:YAG (yttrium aluminum garnet) laser was used for continuous-wave PL excitation.

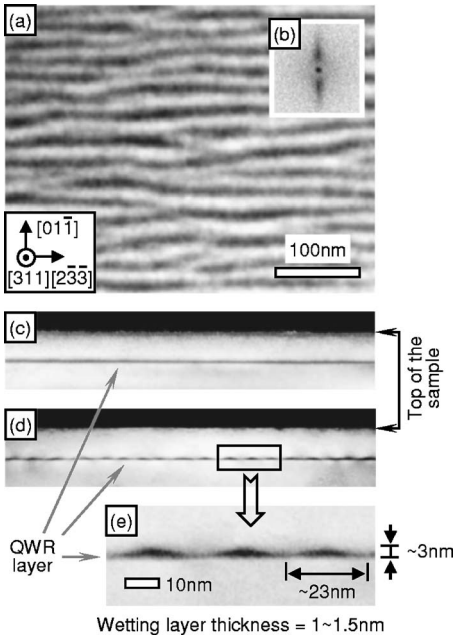

FIG. 1. TEM images of 6-ML InGaAs/GaAs (311)A sample: (a) plan-view TEM from the [311] direction (022 DF condition: strain sensitive), (b) FFT spectrum of (a), (c) X-TEM from the $[01\bar{1}]$ direction (002 DF condition: chemical sensitive), (d) X-TEM from the $[2\bar{3}\bar{3}]$ direction (622 DF condition: chemical sensitive), and (e) enlarged image of part of (c).

The laser spot diameter was ~30 μm and the typical optical excitation power was ~2 mW. The PL signal from the sample was dispersed by a monochromator and detected by a liquid-nitrogen (LN)-cooled optical multichannel analyzer (OMA) V: InGaAs photodiode detector array. In order to eliminate the effect of polarization dependence of the analyzing optics, a quartz depolarizer was inserted along the optical axis during polarized PL measurements.

III. EXPERIMENTAL RESULTS AND DISCUSSION

Low-temperature PL spectra of both samples are plotted in Fig. 2(a). The PL maximum for the 6-ML sample was measured to be at 1.351 eV while the full width at half maximum (FWHM) was 34 meV. Likewise, the PL maximum for the 4-ML sample was 1.438 eV and the FWHM was 16 meV. The larger value of the FWHM for the sample with QWRs is a reflection of the QWR's size distribution. For the polarization measurements the coordinate system is chosen according to Fig. 1. In bulk material the band-edge states are given by an s-like state S_c in conduction band and by three degenerated p-like states X_v, Y_v, and Z_v in the valence band oriented along the $[01\bar{1}]$ (x axis), $[2\bar{3}\bar{3}]$ (y axis), and [311] (z axis) crystallographic directions, respectively. Vertical confinement increases the band gap and removes the degeneracy of the valence band thus splitting all three p states in the (311) QW into the modified $\bar{X}$, $\bar{Y}$, and $\bar{Z}$ states. The lateral confinement along the $[01\bar{1}]$ inherent to the QWRs further modifies the $\bar{X}$, $\bar{Y}$, and $\bar{Z}$ QW states into the $\tilde{X}$, $\tilde{Y}$, and $\tilde{Z}$ QWR states mainly moving the energy of the $\tilde{X}$ state with respect to the energies of the $\tilde{Y}$ and $\tilde{Z}$ states. In case of strong lateral confinement the relative energy positions for the $\tilde{X}$

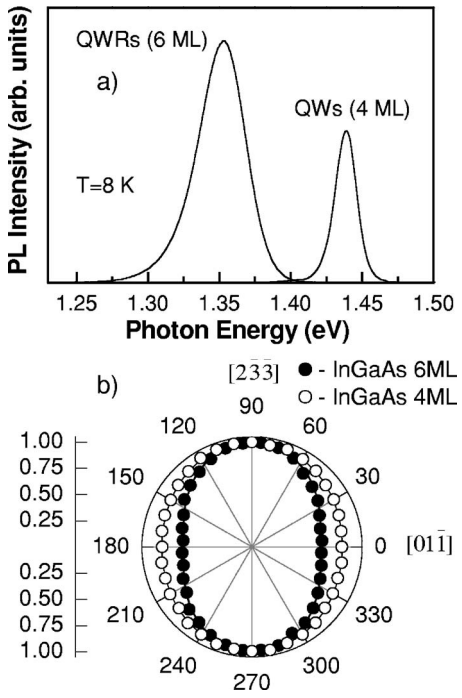

FIG. 2. Low-temperature nonpolarized PL spectra (a) and polar plots of the polarized PL peak intensities of $In_{0.4}Ga_{0.6}As$ (4 ML) QW and $In_{0.4}Ga_{0.6}As$ (6 ML) QWRs on the GaAs(311)A substrate.

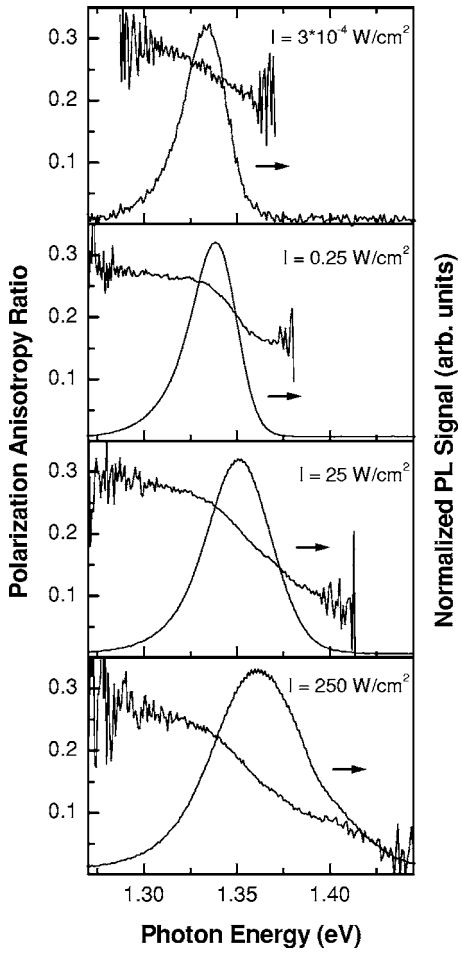

FIG. 3. Normalized PL spectra polarized in the [2$\bar{3}\bar{3}$] direction for the $In_{0.4}Ga_{0.6}As$ (6 ML) QWRs under different PL excitation intensities. The polarization anisotropy ratio changing across the PL band is shown for each excitation intensity.

and $\tilde{Y}$ states can reverse, leading to the observation of temperature-dependent polarization and band-gap anomalies in the strained $Ga_xIn_{1-x}As$ QWR heterostructures.[25] In fact, we find that the dominant polarization switches, indicating that the light-hole and heavy-hole bands cross with increasing temperature if the sample is warmed from 77 to 300 K provided that the pump polarization is parallel to the QWRs.

When spin-orbit coupling is taken into account, there are modifications of the *p*-like orbitals. However, the dominant polarization of the electron-heavy-hole transition remains equal to that between the highest valence band and the *S* state. Following these assignments we have carried out the polarization PL measurements for both samples. Figure 2(b) shows the polar plots of the polarized PL peak intensities for the $In_{0.4}Ga_{0.6}As$ samples with 4 ML (open circles) and 6 ML (closed circles). They show twofold symmetry and are a good fit to the equation $I=A\sin^2(\Psi)+B\cos^2(\Psi)$ with A and B corresponding to the peak intensities of the PL spectra measured along the [2$\bar{3}\bar{3}$] and [01$\bar{1}$] directions, respectively. As it is expected the polarization properties of QWR-like system are pronounced much more distinctly thus pointing out the optical anisotropy of this system. In order to quantify the anisotropy we introduce the polarization anisotropy ratio as $P=(I_{[2\bar{3}\bar{3}]}-I_{[01\bar{1}]})/(I_{[2\bar{3}\bar{3}]}+I_{[01\bar{1}]})$. Figure 3 shows the PL spectral changes observed in the [2$\bar{3}\bar{3}$] polarization under variation of the excitation density. One can also see a significant blueshift of the PL maximum accompanied by an increasing FWHM as the excitation intensity grows. This shift starts before the modification of the high-energy tail of the PL band (normally ascribed to the contribution of the excited states in the QWR spectrum) takes place. PL polarization anisotropy P measured as a function of energy E for each excitation intensity is also shown in Fig. 3. While the $P(E)$ dependence represents the weighted difference of the PL spectra in the polarization directions parallel and perpendicular to the QWR axis, its shape is defined by the spectral shape of the corresponding PL spectra. Therefore, the higher values of the $P(E)$ function at low energies seen in Fig. 3 can be related to a slight shift (~2 meV) of the $I_{[01\bar{1}]}(E)$ maximum to the blue side with respect to the $I_{[2\bar{3}\bar{3}]}(E)$ maximum detected experimentally, and to a change of the low-energy asymmetry of the $I_{[01\bar{1}]}(E)$ and $I_{[2\bar{3}\bar{3}]}(E)$ spectra. The changes of the FWHM and the blueshift in energy of the PL peak for the [2$\bar{3}\bar{3}$] polarization observed in both samples are shown on the logarithmic scale for different excitation densities in Fig. 4. As can be seen from Fig. 4 the blueshift reaches ~25 meV for the $In_{0.4}Ga_{0.6}As$ sample with 6 ML, whereas it is only about of 5 meV in the 4-ML sample at the highest intensities. The FWHM value increases by a factor of 2 in the 6-ML sample (from 28 to 60 meV) and by 40% in the 4-ML sample (from 15 to 24 meV).

There exist various origins of the PL peak shift in the strained QWRs at high excitation density. It can result from (i) an increase of the optical band gap due to the screening of the strain-induced piezoelectric field by the photogenerated

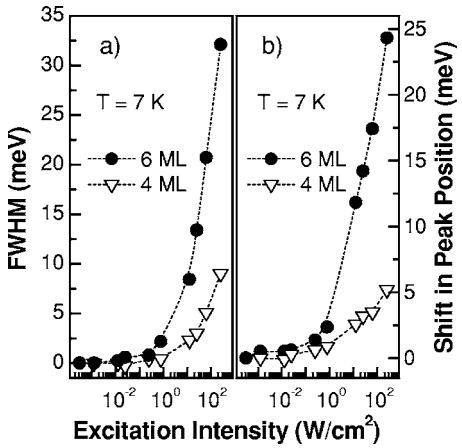

FIG. 4. The changes of the FWHM (a) and a blueshift in energy of the PL peak and (b) for the $[2\bar{3}\bar{3}]$ polarization observed on logarithmic scale for different excitation intensity in $In_{0.4}Ga_{0.6}As$ (4 ML) QW (open triangles) and $In_{0.4}Ga_{0.6}As$ (6 ML) QWRs (closed circles) on the GaAs(311)A substrate. The experimental data connected with dash line for eye guidance.

carriers, (ii) phase-space filling of carriers in QWRs analogous to the Burstein-Moss band filling taking place in bulk semiconductors, and (iii) screening the excitonic correlations and others.

In order to distinguish various contributions in the excitation-density-dependent PL shift and the P value we should make a detailed theoretical calculation of the electronic structure of the system and of the carrier density effects which also takes into account the strain and piezoelectric effects. At the first stage we did not include the piezoelectric fields. The calculation includes the determination of the elastic deformation for the rectangular InGaAs QWR, taking into account the boundary conditions for the high Miller index crystal planes[26] with further finding the energy dispersion and the wave functions for electrons and holes. Since we deal with the optical transitions near the fundamental InGaAs band-gap energy, we assume that the conduction and valence bands are decoupled and the effects of split-off bands are neglected. A simple effective-mass model is used to describe the electron states in the conduction band. In this case the 2D Schrödinger equation has to be solved,

$$\left\{-\frac{\hbar^2}{2}\left[\frac{\partial}{\partial x}\frac{1}{m^*(x,z)}\frac{\partial}{\partial x}+\frac{\partial}{\partial z}\frac{1}{m^*(x,z)}\frac{\partial}{\partial z}\right]+\frac{\hbar^2 k_y^2}{2m^*}+V_d(x,z)+V_c(x,z)\right\}\varphi_i^c(x,z)=\varepsilon_i^c\varphi_i^c(x,z), \tag{1}$$

where the confinement potential $V_c(x,z)$ is a slowly varying function on the scale of the lattice periodicity and $V_d(x,z)$ is the deformation potential of the conduction band. All material parameters necessary for the calculations have been taken from Refs. 27 and 28 and linearly extrapolated for the $In_{0.4}Ga_{0.6}As$ compound. If the coupling of two upper valence bands is solely taking into account the valence-subband states can be analyzed with the Luttinger-Kohn 4×4 Hamiltonian modified by Bockelmann and Bastard,[29]

$$(\hat{H}^L+\hat{H}^s)\varphi_\mu^\nu(x,z)=E\varphi_\mu^\nu(x,z). \tag{2}$$

Here $\hat{H}^L$ is the Luttinger Hamiltonian, $\varphi_\mu^\nu(x,z)$ are the four-component envelope wave functions for holes, and $\hat{H}^s$ is the Pikus and Bir effective strain Hamiltonian[30] that includes the deformation potentials of the valence band. Following the procedure described in Ref. 31 the envelope wave functions in Eqs. (1) and (2) for the electron and hole states in QWR are taken as follows:

$$\varphi^c(x,z)=\frac{1}{\sqrt{L_xL_z}}\sum_l\sum_n\varphi^c(l,n)\exp\{2\pi ilx/L_x\}\exp\{2\pi inz/L_z\} \tag{3}$$

and

$$\varphi_\mu^\nu(x,z)=\frac{1}{\sqrt{L_xL_z}}\sum_l\sum_n\varphi_\mu^\nu(l,n)\exp\{2\pi ilx/L_x\}\exp\{2\pi inz/L_z\}. \tag{4}$$

Here $\mu=\{3/2,1/2,-1/2,-3/2\}$ denotes the components of the hole wave function. Inserting functions (3) and (4) into Eqs. (1) and (2), respectively, we transform these latter into matrix forms, thus allowing the calculation of their eigenvalues and eigenvectors. If one introduces the overlap integrals for the electron and hole envelope wave functions,

$$J_{i,j}^\mu=\int dxdz\varphi_i^{c*}(x,z,k_y)\varphi_{\mu,j}^\nu(x,z,k_y), \tag{5}$$

then the squared transition matrix element for the transitions between the state (i,k_y) of conduction band and the state (j,k_y) of valence band $|M_{i,j}(k_y)|^2$ can be calculated. For the case of linearly polarized light propagating perpendicularly to the plane of QWR it takes the form[29]

$$|M_{i,j}(k_y)|^2=\frac{1}{2}\{|J_{i,j}^{3/2}|^2+|J_{i,j}^{-3/2}|^2\}+\frac{1}{6}\{|J_{i,j}^{1/2}|^2+|J_{i,j}^{-1/2}|^2\}-\frac{1}{\sqrt{3}}\,\mathrm{Re}\{J_{i,j}^{3/2}J_{i,j}^{-1/2}{}^*+J_{i,j}^{1/2}J_{i,j}^{-3/2}{}^*\}\cos 2\vartheta. \tag{6}$$

Here ϑ is the angle between the polarization vector of light and the QWR's axis (y direction). The k_y dependence enters the Eq. (6) through the overlap integrals $J_{i,j}^\mu(k_y)$ [see Eq. (5)]. The spectral dependence of QWR PL is calculated from[19,32]

$$I(\hbar\omega)\propto(\hbar\omega)^2\sum_{i,j}\int_{-\infty}^{\infty}dk_y\int_{-\infty}^{\infty}dE_c\int_{-\infty}^{\infty}dE_v\delta[E_c-E_i^c(k_y)]\times\delta[E_v-E_j^\nu(k_y)]|M_{i,j}(k_y)|^2\times\delta(E_c-E_\nu-\hbar\omega)F(E_c-E_F^c)F(E_\nu-E_F^\nu). \tag{7}$$

Here the 1D density of states in the conduction and valence bands is determined by

$$D^{c,\nu}(E)=\frac{2}{\pi}\sum_l\int_{-\infty}^{\infty}dk_y\delta[E-E_l^{c,\nu}(k_y)], \tag{8}$$

where $E_l^{c,\nu}(k_y)$ are the energy dispersion branches for electrons and holes. The quasi-Fermi energies E_F^c and E_F^ν of the

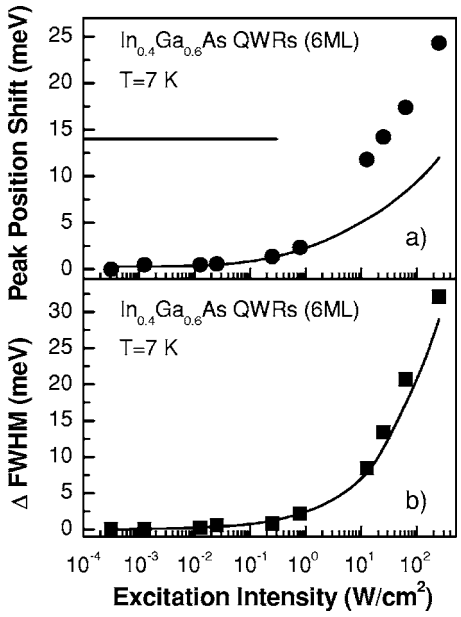

FIG. 5. Blueshift of the PL maximum energy (a) and the change of the PL FWHM (b) vs relative excitation intensity for $In_{0.4}Ga_{0.6}As$ (6 ML) QWRs. Calculated dependences are shown by the solid lines, and the dark circles and squares give experimental results. The horizontal solid line in Fig. 5(a) shows the total redshift ($E_{\max}^{\mathrm{scr}}-E_{\max}^{\mathrm{unscr}}$) of the PL maximum caused by the piezoelectric field with respect to the PL maximum position ($E_{\max}^{\mathrm{unscr}}$) calculated without the piezoelectric effect.

conduction and valence bands are determined from the conditions:

$$n=\int_{-\infty}^{\infty}D^{c}(E)F(E-E_{F}^{c})dE=\int_{-\infty}^{\infty}D^{v}(E)F(E-E_{F}^{v})dE. \tag{9}$$

The Lorentzian broadening function is used instead of the delta function, determining the energy conservation law in Eq. (7), which accounts for the uncertainty due to a finite lifetime of the electron and hole states.

Equations (7)–(9) allow us to calculate the PL intensity for a single QWR. While the difference between the quasi-Fermi-level energies for electrons and holes increases with increasing excitation density, optical transitions with higher energies contribute to the PL spectrum, resulting in a blueshift of the PL peak and its broadening. In order to compare the calculated dependences with the experimental data Eq. (4) has to be convolved with a Gaussian describing the QWR's size distribution in case of a PL spectrum taken at the low excitation density. Putting the approximated relation between the density of excess carriers n_{exc} and the excitation density I_0 to be $n_{\mathrm{exc}}\propto I_0$, the PL intensity $I(\hbar\omega)$ as a function of excitation density is calculated. Figure 5(a) shows the comparison between the calculated and experimental dependences. One can see a good agreement between the results of calculation and experiment for the extended range of the excitation intensities. However, at high intensities the experimentally observed blueshift is more intensive than the calculated one, giving evidence that besides phase-space filling there exist another mechanism giving rise to the efficient complementary blueshift. One possibility is that it can be caused by the screening of the strain-induced piezoelectric field by the photogenerated carriers. Theoretical estimations show[11] that the piezoelectric potential in strained QWRs is in the order of 10 meV and increases with the lateral size of QWR.

In order to estimate the effect of the piezoelectric field screening we assume, following Refs. 5, 14, and 33–35, that the heterostructure is coherent and the thickness of the barrier is much greater than the QWR thickness. Thus, the local elastic strain field ε_{ij} of the structure can be found using the elasticity theory for a plane coherent heterointerface of arbitrary crystallographic orientation.[36] The local elastic strain field results in a piezoelectric polarization field **P**, which is given by $P_i=e_{14}\varepsilon_{jk}$, where e_{14} is the piezoelectric constant. The piezoelectric charge density caused by the presence of a shear component in the strain is $\rho(\mathbf{r})=-\mathrm{div}\,\mathbf{P}(\mathbf{r})$ and includes two different contributions: surface charge at the interfaces due to the discontinuity of polarization vector and volume charge induced by nonhomogeneous strain. In the QW region, far from the wire, the electric field is of 70 kV/cm and parallel to the growth direction. In the QWR the electric field is nonhomogeneous and has other nonzero components. We calculated the electronic structure of the QWR with account of the piezoelectric field for the case of extremely low excitation densities. The total redshift ($E_{\max}^{\mathrm{scr}}-E_{\max}^{\mathrm{unscr}}$) of the PL maximum caused by the piezoelectric field is calculated to be of 14 meV with respect to the PL maximum position ($E_{\max}^{\mathrm{unscr}}$) calculated without the piezoelectric effect. This shift is shown in Fig. 5(a) by a horizontal solid line in the range of low excitation intensities. The magnitude of the shift (14 meV) occurs smaller than that calculated for the strained InGaAs (311)A sidewall QWRs (Ref. 5) (22 meV) being nevertheless significant enough to explain the difference between the experimentally observed PL shift and that calculated with account for the states filling shown in Fig. 5(a). Under elevation of the excitation intensity, the extra free carriers in the QWR screen and the piezoelectric field reduce the excitonic effect due to the screening of the carrier-carrier Coulomb interaction. Finally, the carrier density in the QWR will eventually result in a complete screening of the piezoelectric field and of the excitonic interaction that can be taken into account by neglecting the piezoelectric potential in the single-electron calculations. At very high excitation level, however, new many-body effects can develop making the achievement of a quantitative description very complicated. The investigation of these effects is in progress.

Evidence for the contribution of screening can be gathered by comparing the FWHM calculated within the model of phase-space filling with the experimentally detected FWHM as a function of the excitation intensity. Figure 5(b) shows both dependences on the logarithmic scale. It is seen that the broadening related to the phase-space filling comprises almost the whole FWHM observed experimentally. While the suppression of the piezoelectric field does not lead to further increase of the FWHM, but contrary can even favor the PL band narrowing we conclude that indeed the complementary mechanism of the blueshift is the band-gap enlargement due to screening of the piezoelectric fields by free carriers in QWRs.

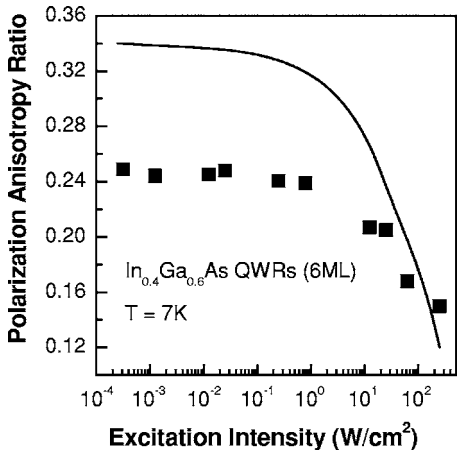

FIG. 6. Polarization anisotropy ratio vs relative excitation intensity for $In_{0.4}Ga_{0.6}As$ (6 ML) QWRs. Calculated dependences are shown by the solid lines, and experimental results are given by the dark squares connected with the dash line for eye guidance.

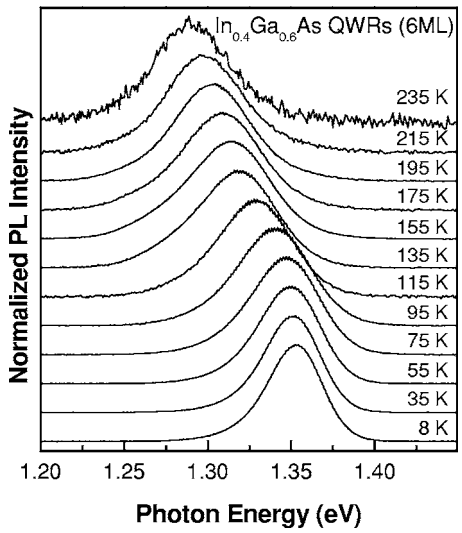

FIG. 7. Normalized PL spectra for $In_{0.4}Ga_{0.6}As$ (6 ML) QWRs measured at different temperatures. For the sake of clarity the spectra are shifted vertically. Lowest temperature is 8 K, all other spectra are measured from 35 K with the $\Delta T = 20-255$ K.

Let us consider the $P(I_0)$ dependence for the QWR system under assumption of phase-space filling. Using Eq. (7) for $\vartheta = 0$ and $\vartheta = \pi/2$ in the squared polarization-dependent transition matrix element $|M_{i,j}(k_y)|^2$ (6) one can calculate $I_{[2\bar{3}\bar{3}]}$ and $I_{[01\bar{1}]}$ intensities for $\mathbf{E}_{[2\bar{3}\bar{3}],[01\bar{1}]}$ being the electric field of emitted light which is detected either along the $[2\bar{3}\bar{3}]$ or $[01\bar{1}]$ direction. The polarization anisotropy ratio P calculated from Eq. (7) is shown in Fig. 6 together with this ratio defined for the PL maximum as a function of the excitation intensity. The behavior of the dependences coincides qualitatively. It is worthy to notice that the calculated dependence is significantly more abrupt than the experimentally measured dependence at high intensities. Therefore if one takes into account the effect of the piezoelectric field screening leading to a more perfect QWR behavior, the difference between the polarization decay rates for the calculated in the approximation of the phase-space filling dependence and for the experimentally measured dependence becomes reasonable.

In our experiments we exclude the temperature heating of the QWR samples under elevation of the excitation density while all measurements have been carried at moderate optical excitation densities. The temperature increase is expected to reveal itself otherwise. Indeed the temperature narrowing of the energy band gap typical for the III-V materials leads to a pronounced redshift of the PL maximum energy. In order to inspect this, the temperature measurements in the $In_{0.4}Ga_{0.6}As$ sample with 6-ML coverage have been carried out at the excitation intensity producing ~15-meV blueshift. The PL spectra are shown in Fig. 7. Total-energy redshift is in the order of ~78 meV if the temperature increases from 8 to 255 K. Such shift is ascribed to the energy-gap shrinking and to the effective carrier transfer from the QWRs of smaller width to the QWRs of larger width at high temperature. The temperature behavior of the polarization anisotropy ratio shown in Fig. 8 is also relevant to the carrier transfer into larger QWRs. The increase of the P value in the temperature interval from 100 to 150 K can be ascribed to the carrier transfer into the QWRs of larger lateral size, producing the higher polarization efficiency. Thus we can resume here that the temperature-induced effects in the PL behavior and the effects arising under the excitation intensity elevation act to some extent in opposite directions in our SILO QWRs. All the effects described above are inherent for the $In_{0.4}Ga_{0.6}As$ sample with 4-ML coverage possessing a noticeable corrugation. However, these effects are less pronounced and serve only to detect the corrugation present in our samples.

IV. CONCLUSIONS

Strain-induced laterally ordered $In_{0.4}Ga_{0.6}As$ on (311)A GaAs template quantum wires have been fabricated and identified with X-TEM technique to be of average length ~1 μm, and an average width and height of 23 and 2 nm, respectively, under InGaAs coverage of 6.0 ML. The photoluminescence spectrum of a sample demonstrates unusually strong optical nonlinearity even at moderate excitation den-

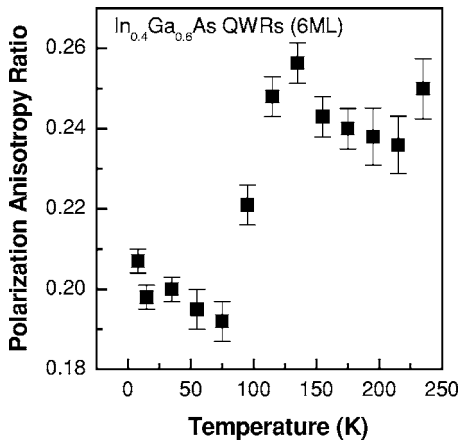

FIG. 8. Temperature dependence of polarization anisotropy ratio $P(T)$ measured for $In_{0.4}Ga_{0.6}As$ (6 ML) QWRs. The increase of the $P(T)$ value in the temperature interval from 100 to 150 K is related to temperature activated carrier transfer into larger QWRs.

sities. The excitonic peak energy blueshifts by ~25 meV without essential contribution of the quantum wire excited states at elevating excitation density. Strong decrease of the polarization anisotropy and increase of the energy of excitonic photoluminescence are attributed to a combined action of the phase-space filling effects and the screening of both the internal piezoelectric field and the Coulomb interaction between carriers. Among other mechanisms contributing to the strong blueshift there could be the decreased transfer of excitons between areas of different monolayer thicknesses within the single-quantum wells, caused by a change in the exciton diffusion from being two dimensional in the quantum wells to one dimensional in the wires.[37] This reduced transfer would result in a blueshift of the peak energy position if the monolayer splitting is unresolved. However, the behavior of the FWHM is expected to be quite different from what we detected in our samples at low temperature. This mechanism due to carrier localization will result in the FWHM broadening at the temperature decrease and should be ruled out here. The blueshift can be related to the many-body effects acting in opposite directions: an attractive interparticle interaction and a repulsive part related to the Pauli exclusion principle governing the behavior of the electrons and holes forming the excitons.[38] A blueshift of homogeneously broadened lines becomes of a detectable value at relatively low exciton densities and much below the Mott density in our QWR structures. However, this blueshift is too small (~1 meV) (Ref. 39) to influence our findings. Finally, we demonstrate the existence of interesting excitation and temperature-dependent polarization anisotropy and strong blueshift in PL coming from the SILO QWRs that gives evidence for the strong nonlinear optical effects.

ACKNOWLEDGMENT

The authors acknowledge the financial support of the National Science Foundation of US through Grant No. DMR-0080054.

[1] R. Nötzel, M. Ramsteiner, Z. Niu, L. Däweritz, and K. H. Ploog, Physica E (Amsterdam) **2**, 979 (1998).
[2] P. O. Vaccaro, M. Hirai, K. Fujita, and T. Watanabe, J. Phys. D **29**, 2221 (1996).
[3] C. Constantin, E. Martinet, F. Lelarge, K. Leifer, A. Rudra, and E. Kapon, J. Appl. Phys. **88**, 141 (2000).
[4] X. Y. Wang, Z. M. Wang, V. R. Yazdanpanah, G. J. Salamo, and M. Xiao, J. Appl. Phys. **95**, 1609 (2004).
[5] D. Alderighi *et al.*, Appl. Phys. Lett. **84**, 786 (2004).
[6] M. Walther, E. Kapon, C. Caneau, D. M. Hwang, and L. M. Schiavone, Appl. Phys. Lett. **62**, 2170 (1993).
[7] R. Rinaldi, A. Passaseo, M. De Giorgi, C. Turco, M. Devittorio, D. Cannoletta, and R. Cingolani, Surf. Sci. Spectra **42**, 7 (1998).
[8] C. Weisbuch and B. Vinter, *Quantum Semiconductor Structures* (Academic, Boston, MA, 1991).
[9] W. R. Tribe *et al.*, Appl. Phys. Lett. **70**, 993 (1997).
[10] U. Bockelmann and G. Bastard, Europhys. Lett. **15**, 215 (1991).
[11] M. Grundmann, O. Stier, and D. Bimberg, Phys. Rev. B **50**, 14187 (1994).
[12] E. Martinet, M.-A. Dupertuis, F. Reinhardt, G. Biasiol, O. Stier, M. Grundmann, D. Bimberg, and E. Kapon, Phys. Rev. B **61**, 4488 (2000).
[13] M. Notomi, J. Hammersberg, J. Zeman, H. Weman, M. Potemski, H. Sugiura, and T. Tamamura, Phys. Rev. Lett. **80**, 3125 (1998).
[14] M. Ilg, K. H. Ploog, and A. Trampert, Phys. Rev. B **50**, 17111 (1994).
[15] P. V. Santos, H.-P. Schnherr, R. Nötzel, and K. H. Ploog, Phys. Status Solidi A **175**, 33 (1999).
[16] K. H. Wang, M. Bayer, A. Forchel, P. Ils, S. Benner, H. Haug, P. Pagnod Rossiaux, and L. Goldstein, Phys. Rev. B **53**, R10505 (1996).
[17] R. Rinaldi, R. Cingolani, L. De Caro, M. Lomascolo, M. DiDio, L. Tapfer, U. Marti, and F. K. Reinhart, J. Opt. Soc. Am. B **13**, 1031 (1996).
[18] E. Martinet, F. Reinhardt, A. Gustafsson, G. Biasiol, and E. Kapon, Appl. Phys. Lett. **72**, 701 (1998).
[19] Y. Tang, H. T. Lin, D. H. Rich, P. Colter, and S. M. Vernon, Phys. Rev. B **53**, R10501 (1996).
[20] T. Baba, T. Hamano, F. Koyama, and K. Iga, IEEE J. Quantum Electron. **28**, 1310 (1992).
[21] P. O. Vaccaro, K. Fujita, and T. Watanabe, Jpn. J. Appl. Phys., Part 1 **36**, 1948 (1997).
[22] H. Wen, Z. M. Wang, and G. J. Salamo, Appl. Phys. Lett. **84**, 1756 (2004).
[23] W. Q. Ma, R. Nötzel, H. P. Schonherr, and K. H. Ploog, Appl. Phys. Lett. **79**, 4219 (2001).
[24] J. Tersoff and R. M. Tromp, Phys. Rev. Lett. **82**, 2782 (1993).
[25] D. E. Wohlert and K. Y. Cheng, Appl. Phys. Lett. **76**, 2247 (2000).
[26] L. De Caro and L. Tapfer, Phys. Rev. B **48**, 2298 (1993).
[27] O. Madelung, *Semiconductor-Basic Data* (Springer, New York, 1986), p. 141.
[28] T. Yamauchi, T. Takahashi, J. N. Schulman, and Y. Arakawa, IEEE J. Quantum Electron. **29**, 2109 (1993).
[29] U. Bockelmann and G. Bastard, Phys. Rev. B **45**, 1688 (1992).
[30] G. E. Pikus and G. L. Bir, *Symmetry and Strain Induced Effects in Semiconductors* (Wiley, New York, 1974).
[31] G. A. Baraff and D. Gershoni, Phys. Rev. B **43**, 4011 (1991).
[32] P. Y. Yu and M. Cardona, *Fundamentals of Semiconductors* (Springer, Berlin, 2001).
[33] P. O. Vaccaro, K. Tominaga, M. Hosoda, K. Fujita, and T. Watanabe, Jpn. J. Appl. Phys., Part 1 **34**, 1362 (1995).
[34] M. Lomascolo *et al.*, J. Phys.: Condens. Matter **11**, 5989 (1999).
[35] D. Alderighi *et al.*, Physica E (Amsterdam) **23**, 449 (2004).
[36] L. De Caro and L. Tapfer, J. Appl. Phys. **79**, 9188 (1996).
[37] A. Gustafsson, X. Liu, I. Maximov, L. Samuelson, and W. Seifert, Appl. Phys. Lett. **62**, 1709 (1993).
[38] N. Peyghambarian, H. M. Gibbs, J. L. Jewell, A. Antonetti, A. Migus, D. Hulim, and A. Mysyrowicz, Phys. Rev. Lett. **53**, 2433 (1984).
[39] V. Voliotis, T. Guillet, R. Grousson, M. Menant, J. Bellessa, X. L. Wang, and M. Ogura, Phys. Status Solidi A **190**, 735 (2002).